Depth-dependent attenuation structure of the inner core inferred from short-period Hi-net data

T. Kazama*, H. Kawakatsu, N. Takeuchi

Earthquake Research Institute, The University of Tokyo, 1-1-1 Yayoi, Bunkyo-ku, Tokyo 113-0032, Japan

ARTICLE INFO

ABSTRACT

Depth-dependent attenuation structure in the inner core below the northeast Pacific is studied utilizing the short-period Hi-net data. The commonly used method of estimating inner core attenuation (differential spectral slope analysis) is not suitable because it is too sensitive to the presence of small amplitude phases. Instead, we found that the method of relative and differential amplitudes is more robust estimator of inner core attenuation. We use the relative amplitude of PKIKP (DF) to PKPs (BC or AB) around 1.0 Hz to estimate t^* as a function of the epicentral distance. Geometrical ray theory was employed to correct the source and propagation effects except that of inner core attenuation. The resulting t^* for South American events shows a clear peak around an epicentral distance of 152°, whose corresponding bottoming depth is about 300 km below the inner core boundary (ICB). This pattern can be explained by a low Q_P (<200), high attenuation region in a depth range of 200–300 km. We also found that, in this depth range, there exists positive correlation between attenuation and velocity, indicating seismic scattering due to anisotropic structure of iron crystals at the intermediate depth of the inner core.

© 2008 Elsevier B.V. All rights reserved.

1. Introduction

The solid inner core's structure has been revealed by observations of core phases, which pass through the Earth's core as compressional body waves (Fig. 1). PKIKP, or DF phase passes through the inner core, whereas PKPs (BC and AB phases) turn in the liquid outer core.

The observed DF phase is more attenuated than BC and AB (Doornbos, 1974), indicating significant anelasticity in the inner core. The cause of the seismic attenuation in the inner core has been attributed to the presence of partial melt; Loper and Fearn (1983) suggested a mushy zone in the inner core, or Singh et al. (2000) suggested spheroidal inclusions of liquid iron. And inner core attenuation has been characterized through its heterogeneity (Cormier and Choy, 1986), anisotropy (Helffrich et al., 2002) and its hemispherical structure (Wen and Niu, 2002; Cao and Romanowicz, 2004) in the inner core.

On the depth dependency of inner core attenuation, several studies have disagreement. Doornbos (1974) showed that the seismic attenuation becomes highest at the top of the inner core and grows lower at deeper depth. In contrast, Morita (1991) found that the attenuation is highest at 200–300 km depth below the ICB. It must be resolved whether these differences come from variations

of analysis methods or inner core heterogeneity (Cormier and Choy, 1986).

In this paper, we studied the depth profile of inner core attenuation. Amplitude analysis method was used, which can estimate inner core attenuation robustly. Our result is consistent with Morita (1991); attenuation is highest at 200–300 km depth below the ICB, not at the uppermost inner core, suggesting attenuation heterogeneity by complex structures in the inner core.

2. Methods of analysis

If a seismic P wave, with the initial amplitude A_0, passes through a medium with the seismic quality factor Q_P, the amplitude spectrum becomes

$$A(f) = A_0 \exp(-\pi f t^*), \tag{1}$$

where

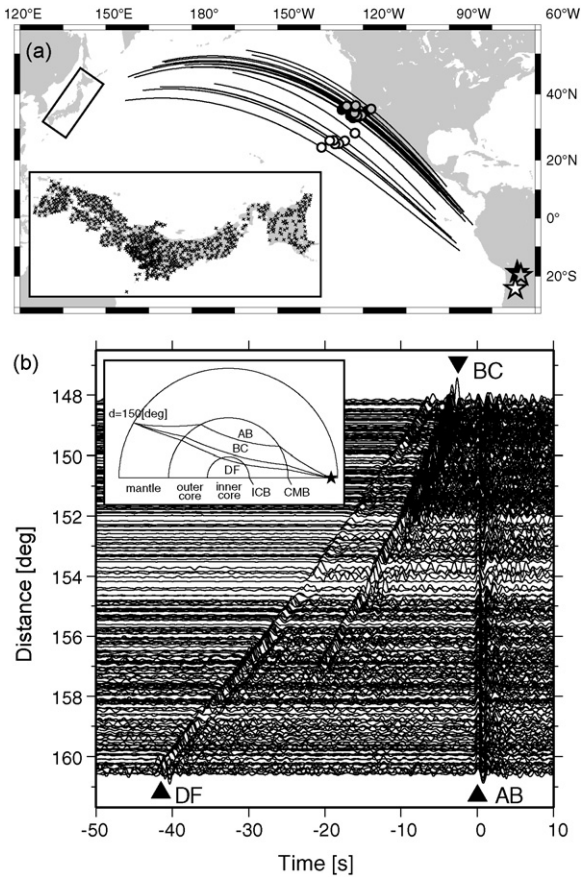$$t^* = \int_{\text{path}} \frac{\mathrm{d}t}{Q_P} \tag{2}$$

is the attenuation factor integrated along the ray path.

2.1. Differential spectral slope method

Assuming that ray paths of core phases in the mantle are similar and that the outer core attenuation is negligible (Buchbinder, 1971),

* Corresponding author.
  E-mail address: takujin@eri.u-tokyo.ac.jp (T. Kazama).

Fig. 1. Core phases. (a) DF ray paths in the inner core (bold lines) with bottoming points (circles). Stars and crosses show hypocenters and Hi-net stations, respectively. Solid, gray and open symbols indicate events 1, 2 and 3 (Table 1), respectively. (b) Core phase waveforms with 1.0 Hz low-pass filter, recorded at Hi-net stations. Each waveform is normalized by AB amplitude and aligned with AB's travel time. Solid curves in the semicircle show ray paths of core phases. Note that waveforms and ray paths are for event 1 (Table 1).
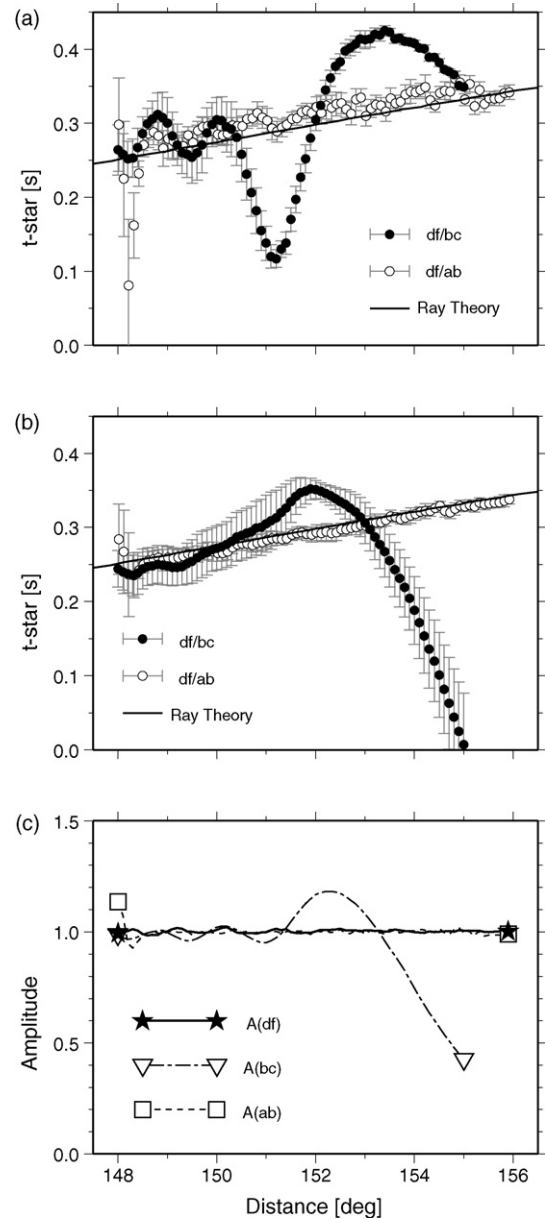
Table 1
Source parameters reported by USGS

	Events		
	1	2	3
Year	2001	2003	2005
Date	June 29	July 27	June 2
UTC	18:35:51	11:41:28	10:55:58
Latitude	−19.473	−19.841	−24.202
Longitude	−66.182	−64.942	−66.863
Depth	276	348	191
Mw	6.1	6.0	6.1
Obs.	383	634	697

Fig. 2. Synthetic tests for DSM waveforms. (a) Slope analysis t^*. (b) Amplitude analysis t^*. In (a) and (b), black and white circles show $t^*_{df/bc}$ and $t^*_{df/ab}$, respectively. (c) Corrected amplitudes of core phases. All of ray theoretical effects, including inner core attenuation, are corrected in this figure. Note that in these figures, source depth is not corrected to 0 km, and that C-cusp is located at 155.0°.

amplitude ratios of core phases can be written as

$$\frac{A_{df}}{A_{ref}} \propto \exp(-\pi f t^*_{df/ref}), \tag{3}$$

where $t^*_{df/ref}$ represents the attenuation in the inner core along the DF path, and the subscript ref indicates a reference phase (AB or BC). Assuming further that Q is independent of frequency, the slope of the logarithmic of spectral ratios gives $t^*_{df/ref}$. This is the most commonly used method of estimating inner core attenuation (e.g., Bhattacharyya et al., 1993; Tseng et al., 2001; Helffrich et al., 2002). Here, we applied this method to the DSM synthetic seismograms (Takeuchi et al., 1996), calculated for the IASP91 velocity model (Kennett and Engdahl, 1991) and the PREM Q-model (Dziewonski and Anderson, 1980). Note that in the modeling, the low velocities of crustal layers are replaced by the velocities of the uppermost mantle to avoid crustal reverberations, and that the source depth and mechanism of the synthetics are based on event 1 (Table 1). Fig. 2 a shows the result of t^*. In this figure, source depth is not corrected, and C-cusp position is located at 155.0°. Both $t^*_{df/bc}$ and $t^*_{df/ab}$ are highly oscillatory and noisy due to the existence of the small PKiKP (CD) phase. The slope analysis is largely affected by phases having small amplitudes, and is not suited for estimating attenuation structure precisely.

2.2. Differential spectral amplitude method

Based on ray theory, core phase amplitudes are affected by geometrical spreading, transmission attenuation at major boundaries, source radiation, and attenuation in the mantle and core. When all of these effects other than that of inner core attenuation are properly corrected, t^* can be also estimated directly from the differential logarithmic amplitude as

$$t^*_{\text{df/ref}}(f) = -\frac{1}{\pi f} \ln \frac{A_{\text{df}}(f)}{A_{\text{ref}}(f)}. \quad (4)$$

Fig. 2 b shows the results for the synthetic seismograms. Here, we corrected the ray theoretical effects with the same structure models as for synthetic waveforms, and averaged $t^*_{\text{df/ref}}(f)$ between 0.4–1.5 Hz to give representative values. Contrary to Fig. 2 a, t^* has smaller error bars and more coherency with the ray theoretical t^*. The CD influences are seen in $t^*_{\text{df/bc}}$: $t^*_{\text{df/bc}}$ at farther than 153.5° deviates by more than 0.1 s from ray theoretical values, indicating poor reproducibility of t^* near C-cusp. If we permit observation error of t^* up to 0.1s, we can use $t^*_{\text{df/bc}}$ estimates except those within 1.5° around C-cusp.

We also checked how accurately the ray theoretical effects are corrected for each core phase as follows. We first corrected all of the ray theoretical effects including inner core attenuation for synthetic core phases, and then plotted amplitude variations of each core phase against the epicentral distance (Fig. 2c). Note that each amplitude is the mean of spectrum amplitudes in a 0.4–1.5 Hz range, and is normalized by an arbitrary value. If ray theory works perfectly, the corrected amplitudes of three phases should stay constant with a same value. Fig. 2c shows that, except for BC phase near the C-cusp, the amplitudes of three phases are nearly constant, proving the efficacy of the amplitude correction based on the ray theory in this frequency range. Although CD influences are still seen in disturbances of BC amplitudes near C-cusp, the oscillatory nature is well predicted by the finite frequency effect of diffracted waves (cf., Aki and Richards, 2002, Fig. 9.36), suggesting a possibility of incorporating this effect for further corrections. Considering these, we suggest that spectral amplitude method can estimate inner core attenuation more robustly than the slope method.

3. Data analysis and results

Short-period seismograms recorded by Japanese Hi-net (Obara et al., 2005) are used for estimating inner core attenuation. We selected three earthquakes at South America (Table 1) with Mw around 6.0 which show good signal-to-noise ratios and simple source time functions. Source depth is deeper than 150 km to avoid interference of depth phases. Fig. 3 shows radiation points of core
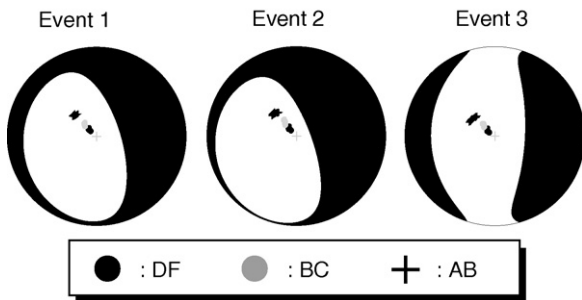

Fig. 3. Radiation points of core phases, with CMT solutions reported by USGS. Solid circles, gray circles and black cross-shapes show radiation points of DF, BC and AB phases, respectively. A gray cross-shape indicates the center of each circle.
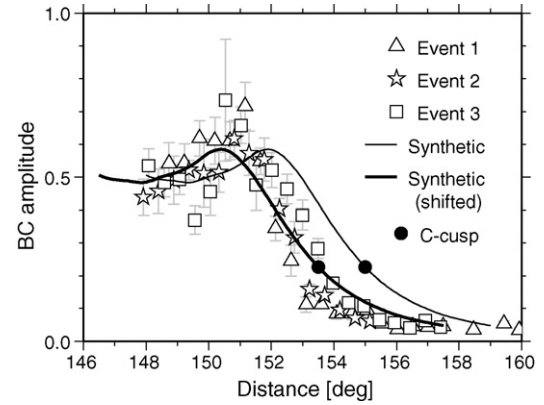

Fig. 4. Variations of BC amplitudes. Open symbols and solid lines show BC amplitudes of three events (Table 1) with source depth corrected to 0 km, and the synthetic amplitudes used in Section 2, respectively. Note that amplitudes of each event are multiplied by a constant value and that the synthetic curve (thick line) is shifted by −1.5° so the variance is minimized at the range of 148–153°.

phases, with CMT solutions reported by USGS. Three core phases radiate close at each focal sphere, suggesting that radiation effects to core phase amplitudes is small. Indeed, t^* values change only by ∼0.01 s, even if other available CMT solutions are used for the source radiation correction.

In Fig. 4, open symbols show observed raw amplitudes of BC phase, averaged over a 0.4–1.5 Hz frequency range. The observed BC amplitudes reach maximum around 150.5° and become smaller at farther distances. Synthetic BC raw amplitudes (thin line), however, are not consistent with the observed amplitudes, suggesting C-cusp position's discrepancy between synthetics and observations. Assuming that the amplitude variation of a phase-branch near the cusp is a function of the distance from the cusp point (Aki and Richards, 2002, *ibid.*), we shift this thin line by every 0.1° so that the synthetic amplitude variation fits with the observed ones at the range of 148–153°. For each event, the amplitude is normalized so as to best fit to the shifted curve. We found that a synthetic curve, shifted by −1.5°, minimizes the variance. The C-cusp location is thus estimated to be at 153.5°, which is consistent with the regional inner core velocity model VMOI (Kaneshima et al., 1994). As discussed in the previous section, we cannot use BC phase amplitudes near the C-cusp because of the CD influence. If we permit < 0.1 s error for t^*, we can trust $t^*_{\text{df/bc}}$ up to 152.0°.

3.1. t^* variations

We applied the spectral amplitude method to the Hi-net data. We cut each core phase with a 4–6 s time window and estimated $t^*_{\text{df/bc}}$ and $t^*_{\text{df/ab}}$ in a frequency range of 0.4–1.5 Hz where S/N ratios are above 2.0. We then averaged t^* for every 1° of epicentral distances for each event.

Fig. 5 a shows t^* variation for event 1 (Table 1). There exists a systematic discrepancy between $t^*_{\text{df/bc}}$ and $t^*_{\text{df/ab}}$, by about 0.25 s at the range of 148–152°. This may imply that amplitudes of core phases are not corrected effectively due to disagreement between reference model and the real Earth. Two possibilities can be considered: Q_P disagreement in the mantle, and/or Q_P's lateral heterogeneity in the lowermost mantle. On the former possibility, assuming higher Q_P, or smaller attenuation in the mantle than PREM, t^* discrepancy (δt^*) becomes smaller. However, no attenuation ($Q_P = \infty$) at the lower mantle (670–2891 km depth) does not match $t^*_{\text{df/bc}}$ and $t^*_{\text{df/ab}}$ (Fig. 5b), suggesting that any 1D Q-model does not account for the t^* discrepancy.
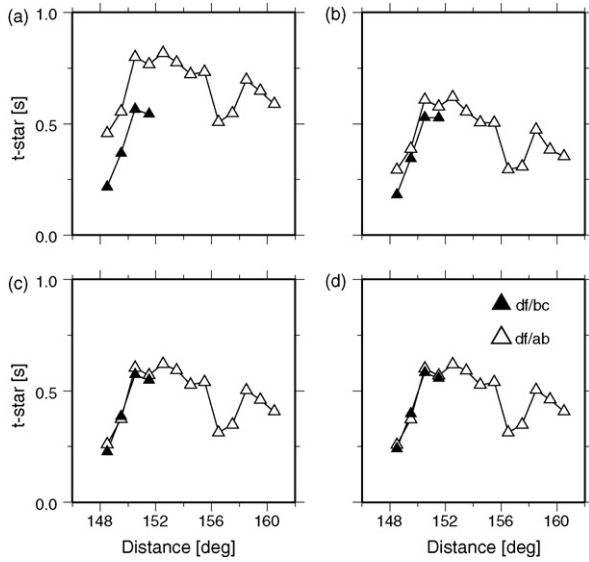
Fig. 5. Averaged t^* variations as a function of epicentral distance for event 1. Core phases are corrected with the PREM mantle Q structure, except for (b) $Q_P = \infty$ in the lower mantle for all phases, (c) $Q_\mu = 220$ in the lower mantle for BC and DF phases, and (d) $Q_\mu = 14$ in 50 km thick layer above the CMB for BC and DF, respectively. Note that source depth (276 km) is not corrected in these figures.

On the latter possibility, if smaller Q_P, high attenuation in the mantle is assumed for DF and BC phases, whose paths are almost same (see semicircle image in Fig. 1b), δt^* becomes smaller. For example, when shear quality factor Q_μ is changed from 312 (PREM) to 220 in the lower mantle, δt^* becomes less than 0.02 s (Fig. 5c). δt^* also becomes smallest, if Q_μ is changed to 14 at 50 km thick above the core–mantle boundary (CMB) (Fig. 5d). Note that Q_P is written as

$$Q_P^{-1} = L Q_\mu^{-1} + (1 - L) Q_\kappa^{-1}, \qquad (5)$$

where $L = (4/3)(V_S/V_P)^2$ and Q_κ represents bulk attenuation. On Fig. 5 c and d, each Q_P value at the lowermost mantle is changed from 820 (PREM) to 585 and 40, respectively. In fact, the lowermost mantle, D″, has lateral heterogeneity (e.g., Kuo et al., 2000). D″ is believed to have small-scale ultra-low velocity zone (ULVZ), whose Q_μ could be less than 3% of PREM's (Fisher et al., 2003). Our DF and BC phases (Fig. 6) might pass through ULVZ at the middle-east side of the Pacific (e.g., Thorne and Garnero, 2004, Fig. 11d), which may explain the systematic shift of t^*.

Here, we corrected amplitudes of core phases, supposing Q_P's lateral heterogeneity in the lowermost mantle; Q_μ at 50 km thick layer above the CMB for DF and BC paths was changed to 14. The final t^* results are shown as Fig. 7, where error bars show t^* distributions. Three events show similar characteristics: t^* increases rapidly by ∼0.4 s for rays bottoming between 200 and 300 km, which is observed for both $t^*_{df/bc}$ and $t^*_{df/ab}$, and decreases slowly by 0.2 s for between 300 and 600 km. Although $t^*_{df/ab}$ after 300 km might still contain the effect of D″ heterogeneity (e.g., Kuo et al., 2000), the consistent variations of $t^*_{df/bc}$ and $t^*_{df/ab}$ shows a robust attenuation nature in the inner core.

3.2. Depth profile of Q_P

The systematic variation of t^* indicates the presence of a high attenuation region in the intermediate depth of the inner core, and we inverted t^* values for a Q_P model. We divided the top of the inner core (600 km thick) into eight layers; each layer is 50 km thick, except that the uppermost and bottom layers are 200 and 100 km
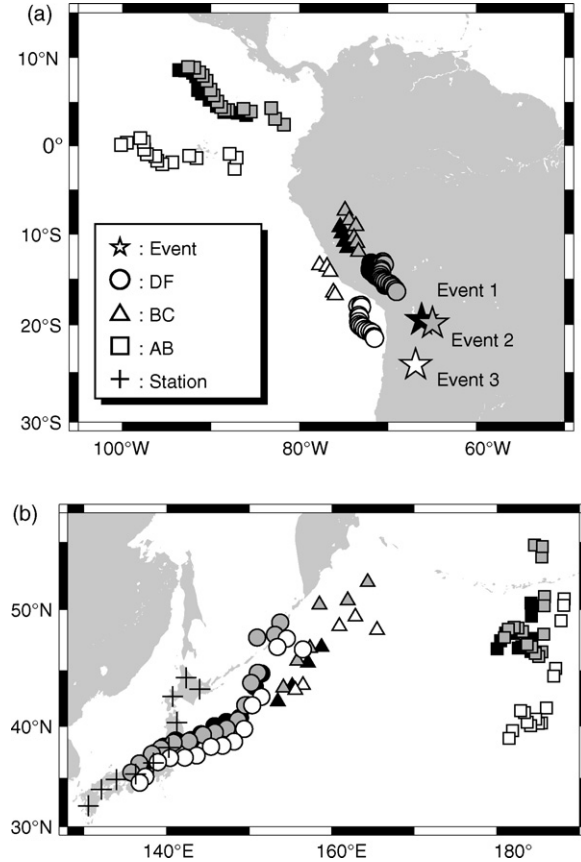
Fig. 6. Piercing points of ray paths of three core phases at the CMB. (a) and (b) Entry and exit points, respectively. Each piercing point is marked with different symbols according to core phases. Solid, gray and open symbols indicate events 1, 2 and 3 (Table 1), respectively.

thick, respectively. The observation equation is written as

$$t_i^* = \sum_{j=1}^{8} \frac{T_i^j}{Q^j} \qquad (6)$$

where T_i^j represents travel time of i-th path in j-th layer. We estimated Q_P structure by employing the conventional least-square method, although the solution may be slightly biased (e.g., Tarantola, 1987).

Fig. 8 b and c shows the results. Q_P at 0–200 km depth in the inner core is ∼350, which is consistent with the result of the same ray paths' analysis (Helffrich et al., 2002). At 200–300 km depth, Q_P value is smaller than 200, and reaches minimum around 275 km ($Q_P \sim 150$). Below 350 km from the ICB, Q_P is greater than 1000, possibly indicating very low attenuation at the lower part of the inner core (Cormier and Li, 2002; Chevrot et al., 2005). Our results suggest extremely high attenuation region between 200 and 300 km below the ICB.

Fig. 8 c compares our Q_P profile with others. Morita (1991) analyzed the same ray paths as ours. He found that Q_P reaches minimum (∼125) at 200–240 km depth, while his application of slope analysis make Q_P structure noisy. Our Q_P model also reach its minimum around 250–300 km, suggesting a characteristic Q_P profile in this region. In contrast, Doornbos (1974) analyzed ray paths from Fiji to Norway, and found Q_P value smallest at the top of the inner core (200) and larger with deeper depth (600 at 400 km), which is consistent with many other studies (e.g., Souriau and Roudil, 1995). However, his result only indicates rough attenuation structure in
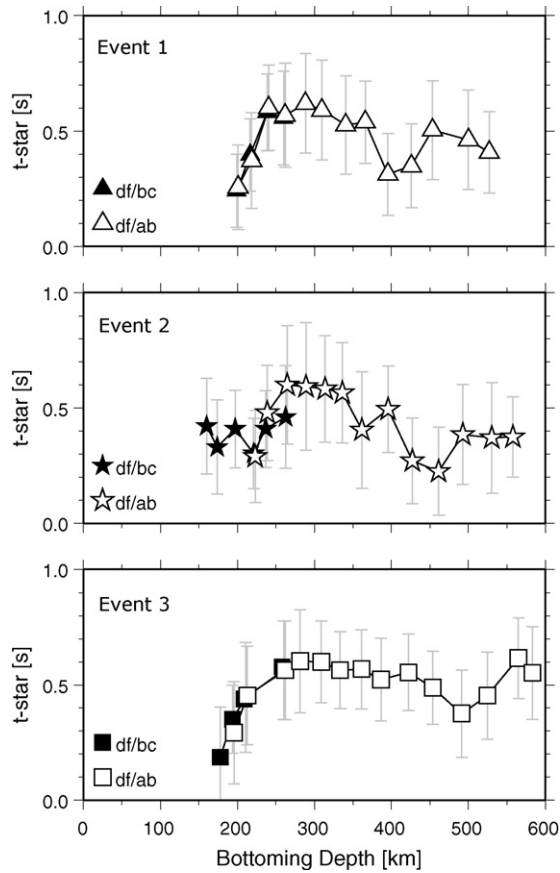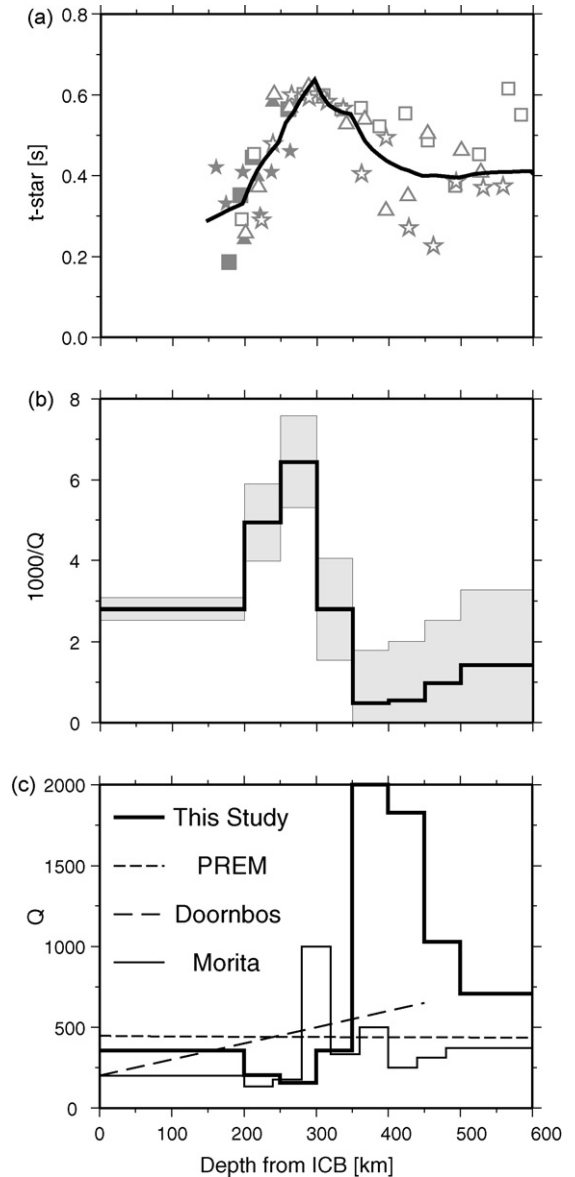
Fig. 7. t^* as the function of DF bottoming depth below the ICB. Black and white symbols represent $t^*_{df/bc}$ and $t^*_{df/ab}$, respectively, and error bars show t^* distributions. Note that systematic discrepancy of $t^*_{df/bc}$ and $t^*_{df/ab}$ (Fig. 5) is corrected, assuming high attenuation at 50 km thick of the lowermost mantle for BC and DF phases. Each graph corresponds with events in Table 1.

the inner core due to the small number of available waveforms. Our Q_P model suggests detailed depth dependency of inner core attenuation owing to the high density of Hi-net array data.

4. Discussions

Inner core attenuation is often studied with the velocity structure of the inner core (e.g., Helffrich et al., 2002; Wen and Niu, 2002; Garcia et al., 2004) to understand the inner core structure. We also estimated inner core V_P structure via travel time residual, $T_{bc} - T_{df}$, which is read from phase peaks of waveforms with a 1.0 Hz low-pass filter. Observed $T_{bc} - T_{df}$ (Fig. 9 a), relative to VMOI (Kaneshima et al., 1994), is about 0.2 s smaller before 150°, and increases gradually after 150°, suggesting negative velocity anomaly at the uppermost inner core and positive anomaly in the intermediate depth of the inner core. This low $T_{bc} - T_{df}$ anomaly is consistent with globally analyzed data (Souriau et al., 2003). (Note that the longitude of the turning point for our ray paths is around 240°, and the angle to the Earth's rotation axis is around 65° (Helffrich et al., 2002).) Then, travel time residuals are inverted for V_P structure, using the same scheme as the Q_P estimator. Fig. 9 b shows the inverted V_P structure with that of PREM and VMOI. V_P anomaly, relative to VMOI, is found to be −0.18% at 0–200 km depth, and +0.25% at 250–350 km depth.

Here we compare our Q_P (Fig. 8) and V_P (Fig. 9) structures with other models. At the uppermost 200 km of the inner core, our V_P value is 0.66% smaller than PREM. Low- V_P structure is often observed at the uppermost inner core for the western hemisphere

Fig. 8. Depth dependency of inner core attenuation. (a) t^* as the function of DF bottoming depth below the ICB. Notation of each symbol is similar with that in Fig. 7. Solid line shows t^* predicted by the Q_P^{-1} model. (b) Q_P^{-1} as a function of inner core depth. Gray shade indicates one standard deviation range. (c) Q_P's depth variation compared with results of other studies. Our attenuation model is shown as a thick line.

(Wen and Niu, 2002; Souriau et al., 2003). Our ray paths just pass through the western hemisphere, and our V_P value illustrates a characteristic structure at the western hemisphere. On the other hand, our Q_P value at the uppermost 200 km is smaller than that of PREM by about 100. A disagreement with our Q_P and the western hemisphere's Q_P by Wen and Niu (2002) may be due to ray paths' difference: DF phases pass through the southwestern part of the inner core for Wen and Niu's and the northwestern part for ours. Our Q_P structure reflects high attenuation at the uppermost region of the northwestern inner core (Helffrich et al., 2002).

Around 250–300 km below the ICB, a positive correlation between attenuation and velocity anomaly can be found: Q_P^{-1} and V_P anomaly relative to PREM are +190% and +0.3% in this region. This positive correlation is often found by global waveform analyses (e.g., Wen and Niu, 2002; Souriau et al., 2003). So far as attenuation is concerned, melt fraction profile in the inner core
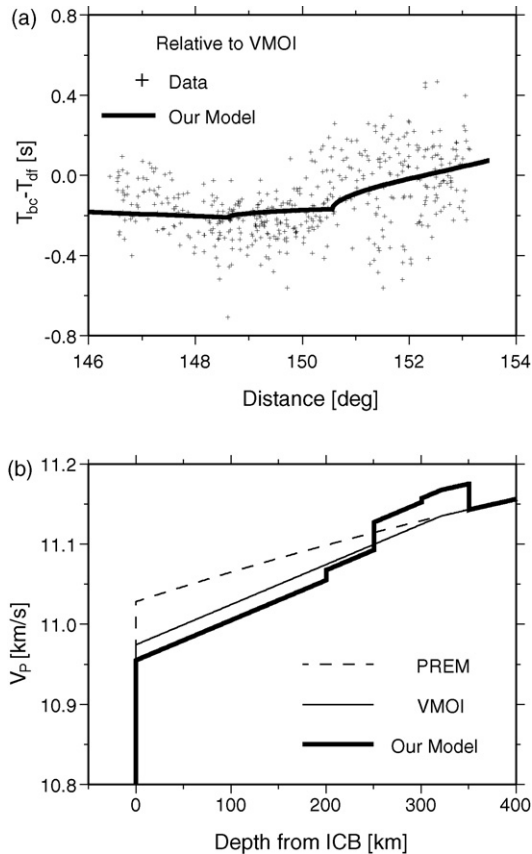
Fig. 9. (a) Travel time residual $T_{bc} - T_{df}$ relative to that of VMOI (Kaneshima et al., 1994). Cross symbols show observed travel time of three events (Table 1). Note that source depth of each event is corrected to 0 km. Synthetic travel time, estimated by a new V_P model (Fig. 9b), is shown by a solid line. (b) V_P variations in the inner core. Thick line shows the inverted model in this study.

by Sumita and Yoshida (2003) may explain our Q_P variation in the inner core; melt fraction reaches maximum at 200 km depth below the ICB, implying the peak of seismic attenuation at the depth. However, it is hardly compatible with the positive correlation between attenuation and velocity.

One possible explanation for the positive correlation is seismic scattering due to anisotropic fabric. Cormier and Li (2002) analyzed global DF waveforms to estimate three dimensional distribution of inner core attenuation due to scattering by a 3D heterogeneous fabric. They suggested that partially aligned iron crystals are responsible for both high Q_P^{-1} and V_P anomalies at the upper half of the inner core. Indeed, our Q_P and V_P variations at 200–300 km depth are very robust owing to high-dense ray paths and the agreement between $t^*_{df/bc}$ and $t^*_{df/ab}$ around 200–300 km depth region. A positive correlation between attenuation and velocity in this region suggests that a viable scattering mechanism might be anisotropic structure in the inner core.

5. Conclusions

We studied the depth dependency of inner core attenuation using high-dense short-period Hi-net data. Synthetic tests showed that commonly used method biases t^* estimation, since the method is sensitive to phases with small amplitudes, and that relative and differential amplitudes are more robust estimators of inner core attenuation. We found high attenuation at 200–300 km depth of the inner core below the northeastern Pacific. In this depth range, attenuation and velocity are found to have positive correlation, implying

that scattering attenuation due to anisotropic fabric could occur in this region.

References

Aki, K., Richards, P.G., 2002. Quantitative Seismology, 2nd ed. University Science Books, 704 pp.
Bhattacharyya, J., Shearer, P., Masters, G., 1993. Inner core attenuation from short-period PKP(BC) versus PKP(DF) waveforms. Geophys. J. Int. 114, 1–11.
Buchbinder, G.G.R., 1971. A velocity structure of the Earth's core. Bull. Seism. Soc. Am. 61, 429–456.
Cao, A., Romanowicz, B., 2004. Hemispherical transition of seismic attenuation at the top of the Earth's inner core. Earth Planet. Sci. Lett. 228, 243–253.
Chevrot, S., Garcia, R.,Tkalcic, H., 2005. A new global PKP data set to study the Earth's deep interior, EOS Trans. AGU 86 (52), Fall Meet. Suppl.: S33D-07.
Cormier, V.F., Choy, G.L., 1986. A search for lateral heterogeneity in the inner core from differential travel times near PKP-D and PKP-C. Geophys. Res. Lett. 13, 1553–1556.
Cormier, V.F., Li, X., 2002. Frequency-dependent seismic attenuation in the inner core. 2. A scattering and fabric interpretation. J. Geophys. Res. 107, 2362.
Doornbos, D.J., 1974. The anelasticity of the inner core. Geophys. J. R. Astron. Soc. 38, 397–415.
Dziewonski, A.M., Anderson, D.L., 1980. Preliminary reference Earth model. Phys. Earth Planet. Inter. 25, 297–356.
Fisher, J.L., Wysession, M.E., Fischer, K.M., 2003. Small-scale lateral variations in D″ attenuation and velocity structure. Geophys. Res. Lett. 30, 1435.
Garcia, R., Chevrot, S., Weber, M., 2004. Nonlinear waveform and delay time analysis of triplicated core phases. J. Geophys. Res. 109, B01306.
Helffrich, G., Kaneshima, S., Kendall, J.-M., 2002. A local, crossing-path study of attenuation and anisotropy of the inner core. Geophys. Res. Lett. 29, 1568.
Kaneshima, S., Hirahara, K., Ohtaki, T., Yoshida, Y., 1994. Seismic structure near the inner core–outer core boundary. Geophys. Res. Lett. 21, 157–160.
Kennett, B.L.N., Engdahl, E.R., 1991. Traveltimes for global earthquake location and phase identification. Geophys. J. Int. 105, 429–465.
Kuo, B.Y., Garnero, E.J., Lay, T., 2000. Tomographic inversion of S-SKS times for shear velocity heterogeneity in D″: Degree 12 and hybrid models. J. Geophys. Res. 105 (28), 139–157.
Loper, D.E., Fearn, D.R., 1983. A seismic model of a partially molten inner core. J. Geophys. Res. 88, 1235–1242.
Morita, Y., 1991. The attenuation structure in the inner-core inferred from seismic body waves (Japanese with English abstracts). In: Yukutake, T. (Ed.), Central Core of the Earth, 1, 65–75.
Obara, K., Kasahara, K., Hori, S., Okada, Y., 2005. A densely distributed high-sensitivity seismograph network in Japan: Hi-net by National Research Institute for Earth Science and Disaster Prevention. Rev. Sci. Instrum. 76, 021301.
Singh, S.C., Taylor, M.A.J., Montagner, J.P., 2000. On the presence of liquid in Earth's core. Science 287, 2471–2474.
Souriau, A., Roudil, P., 1995. Attenuation in the uppermost inner core from broad-band GEOSCOPE PKP data. Geophys. J. Int. 123, 572–587.
Souriau, A., Garcia, R., Poupinet, G., 2003. The seismological picture of the inner core: structure and rotation. C. R. Geosci. 335, 51–63.
Sumita, I., Yoshida, S., 2003. Thermal interactions between the mantle, outer and inner core, and the resulting structural evolution of the core, Earth's core. Geo-dyn. Ser. 31, 213–231.
Takeuchi, N., Geller, R.J., Cummins, P.R., 1996. Highly accurate P-SV complete synthetic seismograms using modified DSM operators. Geophys. Res. Lett. 23, 1175.
Tarantola, A., 1987. Inverse Problem Theory: Methods for Data Fitting and Parameter Estimation. Elsevier, Amsterdam, 613 pp.
Tseng, T.L., Huang, B.S., Chin, B.H., 2001. Depth-dependent attenuation in the uppermost inner core from the Taiwan short period seismic array PKP data. Geophys. Res. Lett. 28, 459.
Thorne, M.S., Garnero, E.J., 2004. Inferences on ultralow-velocity zone structure from a global analysis of SPdKS waves. J. Geophys. Res. 109, B08301.
Wen, L., Niu, F., 2002. Seismic velocity and attenuation structures in the top of the Earth's inner core. J. Geophys. Res. 107, 2273.
Wessel, P., Smith, W.H.F., 1998. New, improved version of the Generic Mapping Tools released. EOS Trans. AGU 79, 579.